Electronic Supplementary Material (ESI) for Journal of Materials Chemistry A.
This journal is © The Royal Society of Chemistry 2022

Supporting Information

Fabrication toward Stable Perovskite Solar Cells with Efficiency over 20% under Open Air via In-situ Polymerized Bi-functional Additive

Lei Ning,[a] Providence Buregeya Ingabire,[a] Ningxia Gu,[a] Pingfan Du,[a] Dongfang Lv,[a] Xiang Chen,[a] Lixin Song,[*a] Wei-Hsiang Chen,[b] Jie Xiong[*a]

[a] College of Textile Science and Engineering, Zhejiang Sci-Tech University, Hangzhou, 310018, China

[b] School of Science, Huzhou University, Huzhou, 313000, Zhejiang, China

Corresponding author Tex: +86 57186843586; E-mail address: lxsong12@zstu.edu.cn (LX Song); jxiong@zstu.edu.cn (J Xiong)

Experimental Sections

Materials: ITO glass (sheet resistance, 12 Ω sq^{-1}) substrates are purchased from Advanced Electronic Technology Co., Ltd. Anhydrous dimethyl sulfoxide (DMSO, 99.7%), isopropanol (IPA, 99.7%), anhydrous dimethylformamide (DMF, 99.8%), anhydrous ethanol (99.7%), acetone (99%), anhydrous chlorobenzene (CB, 99.8%), anhydrous acetonitrile (ACN, 99.5%), anhydrous ethyl acetate (EA, 99.5%), 2, 2'-Azobis(2-methylpropionitrile) (AIBN, 98%), and 2, 2, 2-trifluoroethyl methacrylate (TFEMA, 99.9999%) are all purchased from Aladdin. [6,6]-phenyl-C61-butyric acid methyl ester ($PC_{61}BM$, 99%), Lead (II) iodide (PbI_2, 99.99%), formamidinium iodide (FAI, 99.5%), methylammonium bromide (MABr, 99.5%), lead bromide ($PbBr_2$, 99.99%), cesium iodide (CsI, 99.99%), lithium bis(trifluoromethanesulfonyl)imide (Li-TFSI, 99.95%), 4-tert-butylpyridine (TBP, 98%), and spiro-OMeTAD (99.5%) are bought from Xi'an Polymer Light Technology Corp. SnO_2 colloidal solution (15% in water) was purchased from Alfa Aesar. All chemicals are used without any further purification.

Solar cell device fabrication: ITO glass substrates are first sequentially cleaned with detergent, deionized water, acetone, and ethanol for 20 min each in an ultrasonic bath. The glass substrates are then dried in the hot plate and cleaned by an ultraviolet ozone treatment for 45 min before use. 0.2 mL of SnO_2 colloidal solution is diluted in 1.2 mL of deionized water (mass ratio, 2.14 wt%) and then drips on the pre-cleaned ITO glasses at a rate of 4000 rpm for 30 s, followed by thermal annealing treatment at 150 °C for 30 min in air condition. When it is cooled down to room temperature, the glass substrates are extra treated by ultraviolet ozone for 15 min. The $Cs_{0.05}(FA_{0.83}MA_{0.17})_{0.95}Pb(I_{0.83}Br_{0.17})_3$ perovskites are fabricated by dissolving a 95% (volume ratio) precursor solution of PbI_2 (1.1 M), FAI (1 M), $PbBr_2$ (0.2 M), and MABr (0.2 M) in a solution of anhydrous DMF: DMSO = 4:1 (volume ratio) and 5% (volume ratio) CsI from a 1.5 M stock solution in DMSO. The as-prepared perovskite precursor solution is spin-coated by a two-step program at 2000 rpm for 10 s and 4000 rpm for 30 s. Approximately 245 μL EA is rapidly dropped on the center of substrate 15 s prior to the end of the program, the as-prepared perovskite film is

heated at 100 °C for 5 min and then placed at 150°C for 20 min to achieve an in-situ polymerization strategy. For the crosslinked perovskite samples, the 1.2 mg TFEMA monomers and 0.3 mg AIBN initiators are dissolved in 1 mL antisolvent. After cooled to room temperature, 60 μL of spiro-OMeTAD solution, which consists of 72.3 mg spiro-OMeTAD, 28.8 μL of TBP, and 17.5 μL of Li-TFSI solution (520 mg Li-TSFI dissolve in 1 mL ACN) in 1 mL of chlorobenzene, is spin-coated on the top of the perovskite films at a rate of 3000 rpm for 30 s. Finally, an Ag electrode with a thickness of 80 nm is deposited by thermal evaporation. The active area of this electrode is fixed at 0.06 cm^2. All devices are assembled in the ambient environment (20-30% relative humidity) at room temperature (20-25 °C).

Material characterization: X-ray photoelectron spectroscopy (XPS, K-Alpha, USA) is performed using a micro-focus monochromatic Al Kα X-ray source, which is corresponded to the instrument resolution of 0.45 eV. Fourier transform infrared (FTIR) spectrum is recorded using Nicolet 5700 Fourier Transform Infrared Spectrometer. X-ray diffraction pattern (XRD, Thermo Fisher Scientific) is measured with Cu Kα radiation using in an angle range and scan rate of 5-50 ° and 3 °/min, respectively. Top-view scanning electron microscopy (SEM) images and energy dispersive X-ray spectroscopy (EDS) analysis are collected using a scanning electron microscope (Zeiss SUPRA 55) with an electron beam accelerated voltage at 3 kV, enabling operation at a variety of currents. The absorption spectra of the perovskite films are collected by ultraviolet and visible spectrophotometry (UV-vis, P4, China). The steady-state photoluminescence (PL) spectrum is measured by Fluo Time 300 fluorophotometer Lifetime Spectrometer with an excitation wavelength of 520 nm. Time-resolved PL (TRPL) decay is carried out using a picosecond diode laser with an excitation wavelength of 780 nm. The electrochemical impedance spectroscopy (EIS) is measured by a potentiostat (Im6ex/Zahner) to explore charge transfer properties and battery performance with an alternative signal amplitude of 10 mV and a frequency range of 0.01-100 kHz. The contact angle of water droplets on surfaces of perovskite film is recorded by a contact angle measurement instrument (Fangrui, Shanghai). Incident photo-to-current conversion efficiency (IPCE) curves are

recorded using a quantum efficiency (QE)/IPCE measured system (Solar Cell Scan 100/Zolix) and calibrated by a monocrystalline silicon diode. Thermogravimetric analysis (TGA, China) is conducted under nitrogen atmosphere.

^{1}H and ^{13}C Nuclear Magnetic Resonance. The high-resolution liquid NMR spectrometer is measured by Bruker AVANCE (500 MHz). The samples for NMR measurement are dissolved into a solution of DMSO-d6 but with a higher content of the TFEMA dimers to increase the signals of the characteristic functional groups.

The current density versus voltage (J-V) curves of the devices are measured by a Keithley 2400 Sourcemeter with a solar simulator (USA) under 100 mW cm^{-2} illumination (AM 1.5 G irradiation).

The PL decay curves are fitted to a bi-exponential rate law:

$$Y = A_1 \exp\left(-\frac{t}{\tau_1}\right) + A_2 \exp\left(-\frac{t}{\tau_2}\right) + y_0 \quad \text{(S1)}$$

where A_1 and A_2 are the relative amplitudes and τ_1 and τ_2 represent the carrier lifetimes for the fast and slow recombination, respectively.

And the average TRPL lifetime is calculated by the equation:

$$\tau_{ave} = \frac{A_1 * \tau_1^2 + A_2 * \tau_2^2}{A_1 * \tau_1 + A_2 * \tau_2} \quad \text{(S2)}$$

He I (hν = 21.22 eV) emission source is employed and the helium pressure in the chamber during analysis about 2×10^{-8} mbar. The work function (W_F) of perovskite single crystals can be calculated from the following equation:

$$W_F = h\nu - (E_{Fermi} - E_{Cutoff}) \quad \text{(S3)}$$

where the E_{cutoff} is the steep edge position of the test film in the UPS spectrum. The valence band (E_V) and conduction band (E_C) of the film sample can be calculated by the

$$E_V = W_F + VBM \quad \text{(S4)}$$

$$E_C = W_F + VBM - E_g \quad \text{(S5)}$$

where the VBM is the valence band maximum, and the E_g is the bandgap calculated by UV-vis measurements.

The light-intensity-dependent open-circuit voltage is measured to characterize the carrier recombination mechanisms within the PSCs. The results are fitted using the following equation:

$$n = \frac{q \quad dV_{oc}}{kTd(ln\varphi)} \tag{S6}$$

where k is the Boltzmann constant, T is the temperature in kelvin, and q is the elementary charge.[1, 2]

The dark J-V measurements of the electron-only transport cells is used to investigate the defect density and electron mobility of the perovskite films. The trap filled limit voltages (V_{TFL}) is estimated by linear fitting of the I-V responses. The trap density is calculated using the following equation:

$$N_{defects} = \frac{2\ \varepsilon_0 \varepsilon_r V_{TFL}}{eL^2} \tag{S7}$$

where ε_0 is the permittivity of the free space, ε_r is the relative dielectric constant (~28), e is the electron charge, and L is the thickness of the perovskite layer (~500 nm).[3, 4]

The charge mobility of the perovskite films with and without the in-situ cross-linking process are measured using the Mott-Gurney equation:

$$J = \frac{9V_{TFL}^2 \mu \varepsilon_0 \varepsilon_r}{8L^3} \tag{S8}$$

where J is the current density and μ is the charge mobility.

The hysteresis index of the PSCs is calculated by the following equation:

$$Hysteresis\ index\ = \frac{PCE_{Reverse} - PCE_{Forward}}{PCE_{Reverse}} \times 100\% \tag{S9}$$

The crosslinking process of the TFEMA dimers:

1. Initiator decomposition

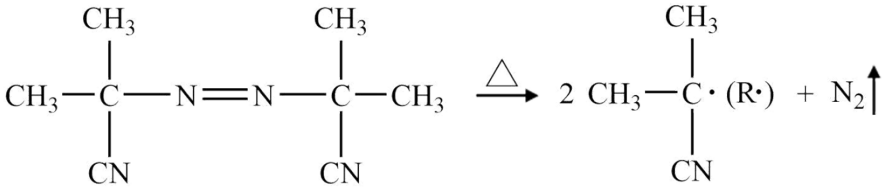

2. Chain initiation

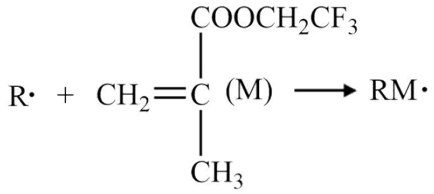

3. Chain growth

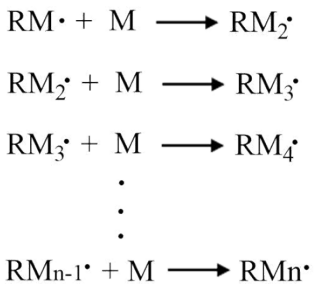

4. Chain termination

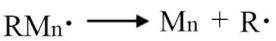

The initiators are first promoted to an excited singlet state by heating at 150 ℃ to become radicals (1), which combine with TFEMA monomers (2), and bridge with adjacent monomers units to provide new alkyl radicals that propagates into long-chain polymers (3). The obtained composites stop crosslinking to form bulkier polymers when two chain radicals interact with each other and then the R· binds to the TFEMA monomers to start a new reaction (4).

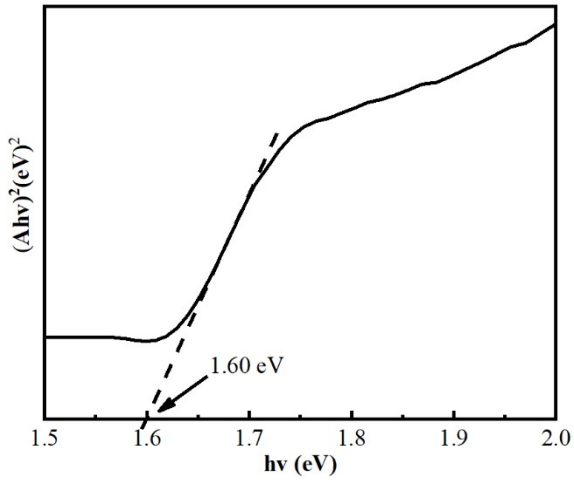

Figure S1. Tauc plot of perovskite thin film. The line indicates a bandgap of about 1.60 eV.

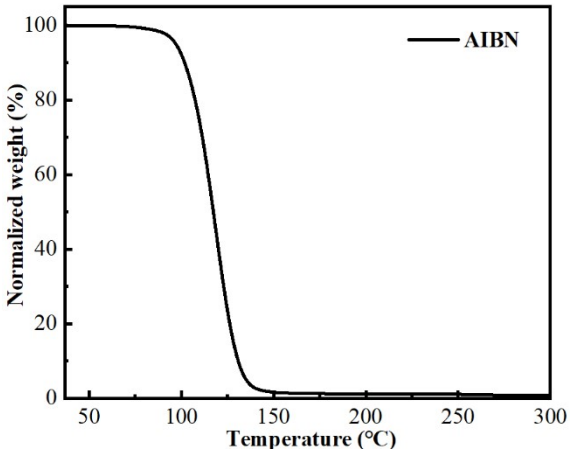

Figure S2. Thermogravimetric analysis of the initiator (AIBN).

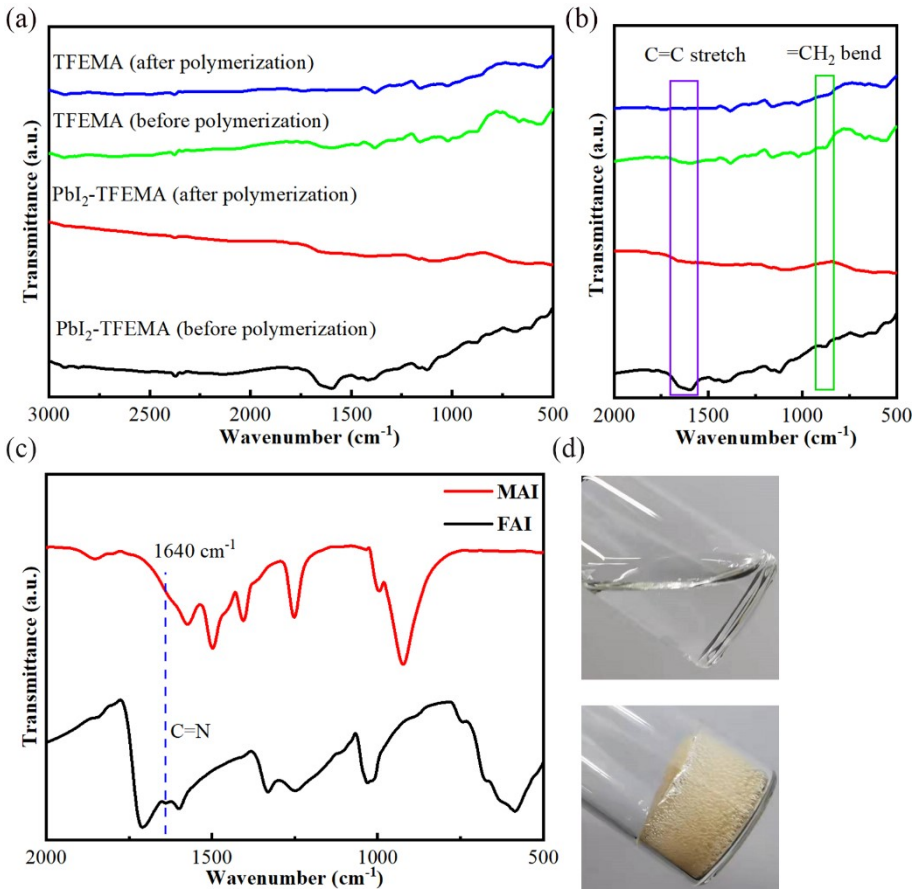

Figure S3. (a) FTIR spectra of the TFEMA monomers, TFEMA dimers, PbI_2-TFEMA film before and after the in-situ polymerization process. (b) Magnification of the corresponding scale between 500 and 2000 cm^{-1}. (c) FTIR spectra of the MAI and FAI powder. (d) Photographs of the TFEMA monomers (the top) and the TFEMA dimers (the bottom) after thermal annealing treatment (100 ℃ for 5 min and 150 ℃ for 20 min).

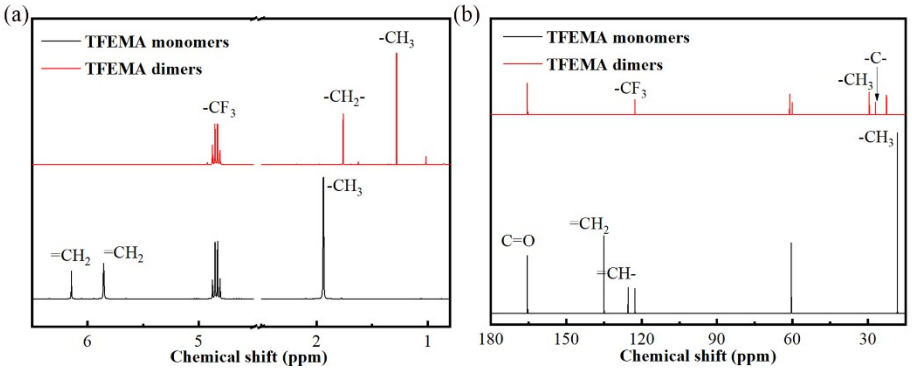

Figure S4. Liquid-state (a) ^{1}H and (b) ^{13}C NMR spectra of solutions with the TFEMA monomers and dimers collect in DMSO-d6.

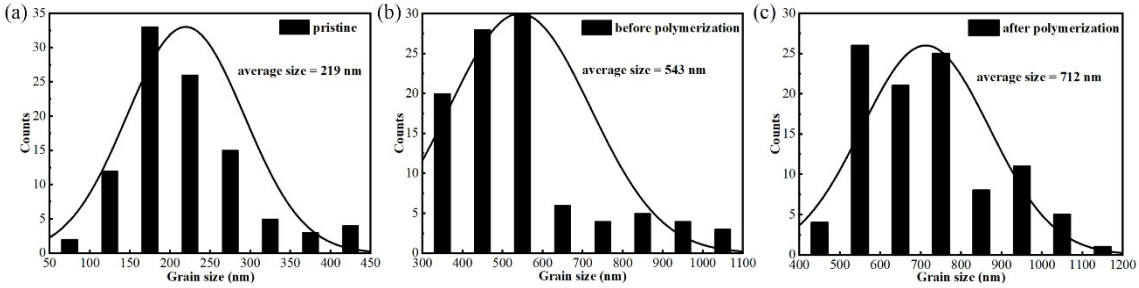

Figure S5. Histogram of grain size distributions for perovskite films of (a) pristine, (b) the TFEMA monomers, and (c) the TFEMA dimers.

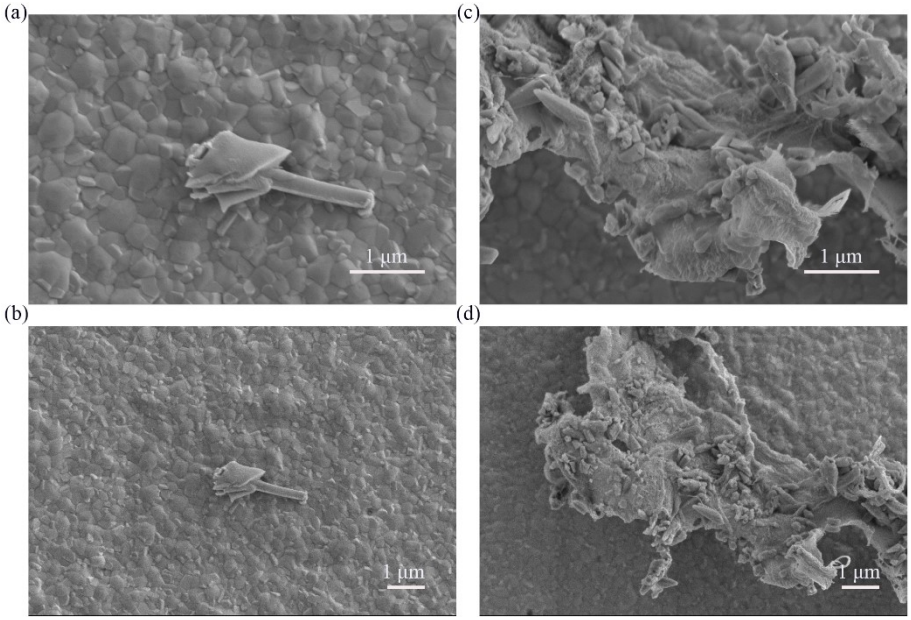

Figure S6. Top-view SEM images with different concentrations of the TFEMA dimers. (a, b) Low concentration (1.2 mg/mL) of the TFEMA monomers polymerized at the top of the perovskite film. (c, d) High concentration (2 mg/mL).

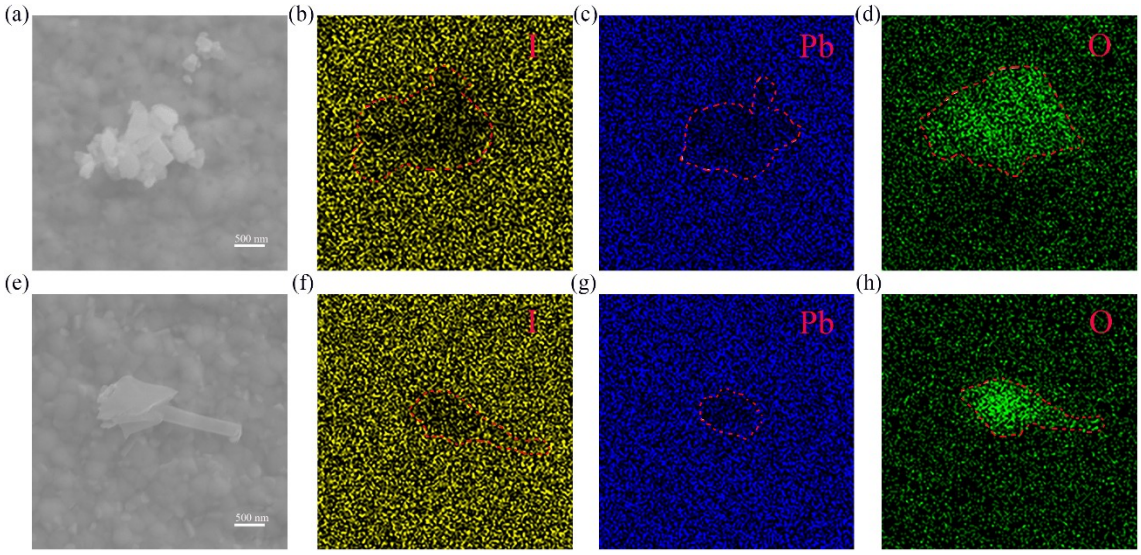

Figure S7. EDS elemental distribution maps of the perovskite films. (a) The film with high concentration of the TFEMA dimers (2 mg/mL) and the corresponding elemental mapping of (b) I, (c) Pb, and (d) O element, respectively. (e) The optimized film and the corresponding elemental mapping of (f) I, (g) Pb, and (h) O element, respectively.

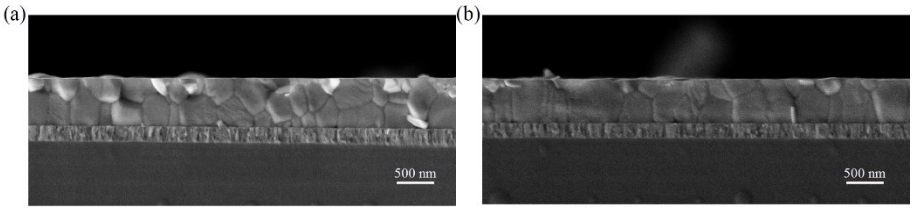

Figure S8. Cross-sectional SEM images of the perovskite films treatment (a) without and (b) with the TFEMA dimers.

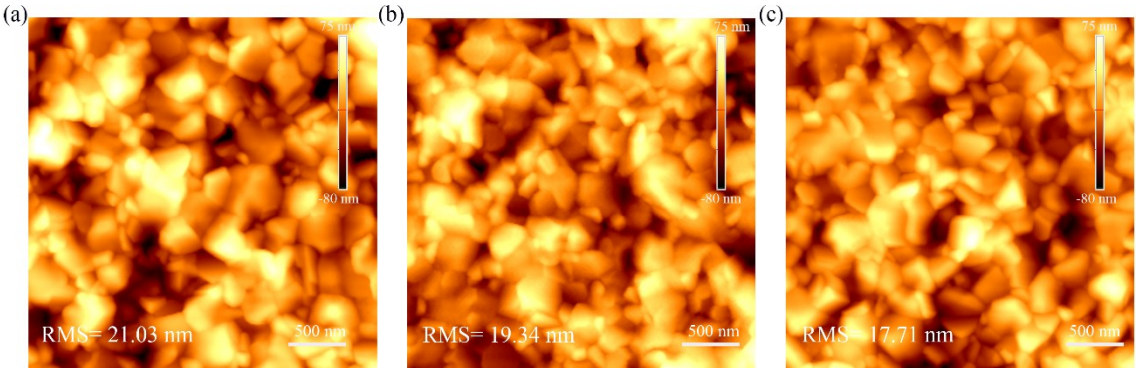

Figure S9. AFM analysis of (a) the pristine film, (b) the TFEMA-monomers-treated film, and (c) the TFEMA-dimers-optimized perovskite film.

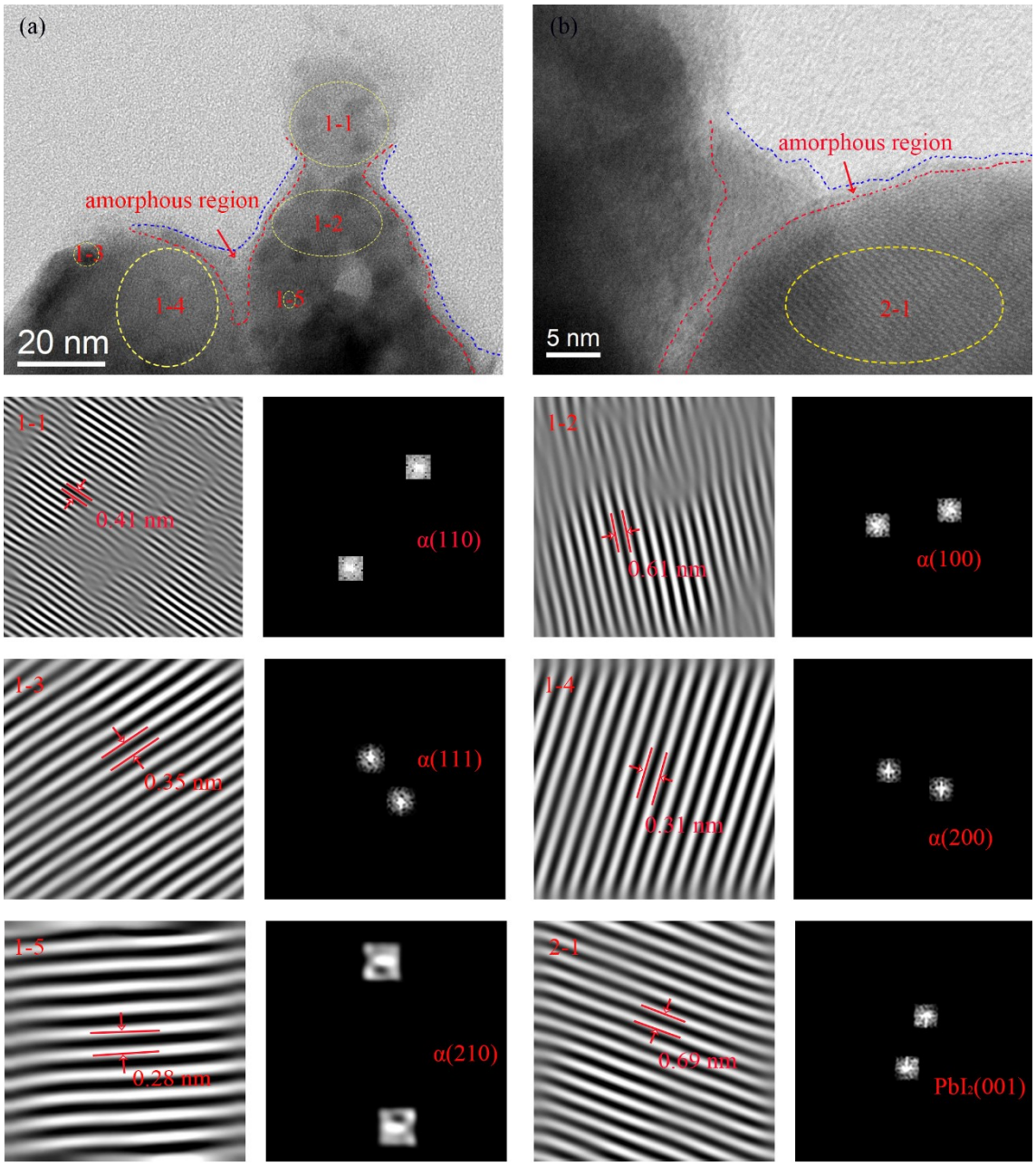

Figure S10. (a, b) HRTEM images and the corresponding FFT analysis of the perovskite sample after an in-situ crosslinking strategy.

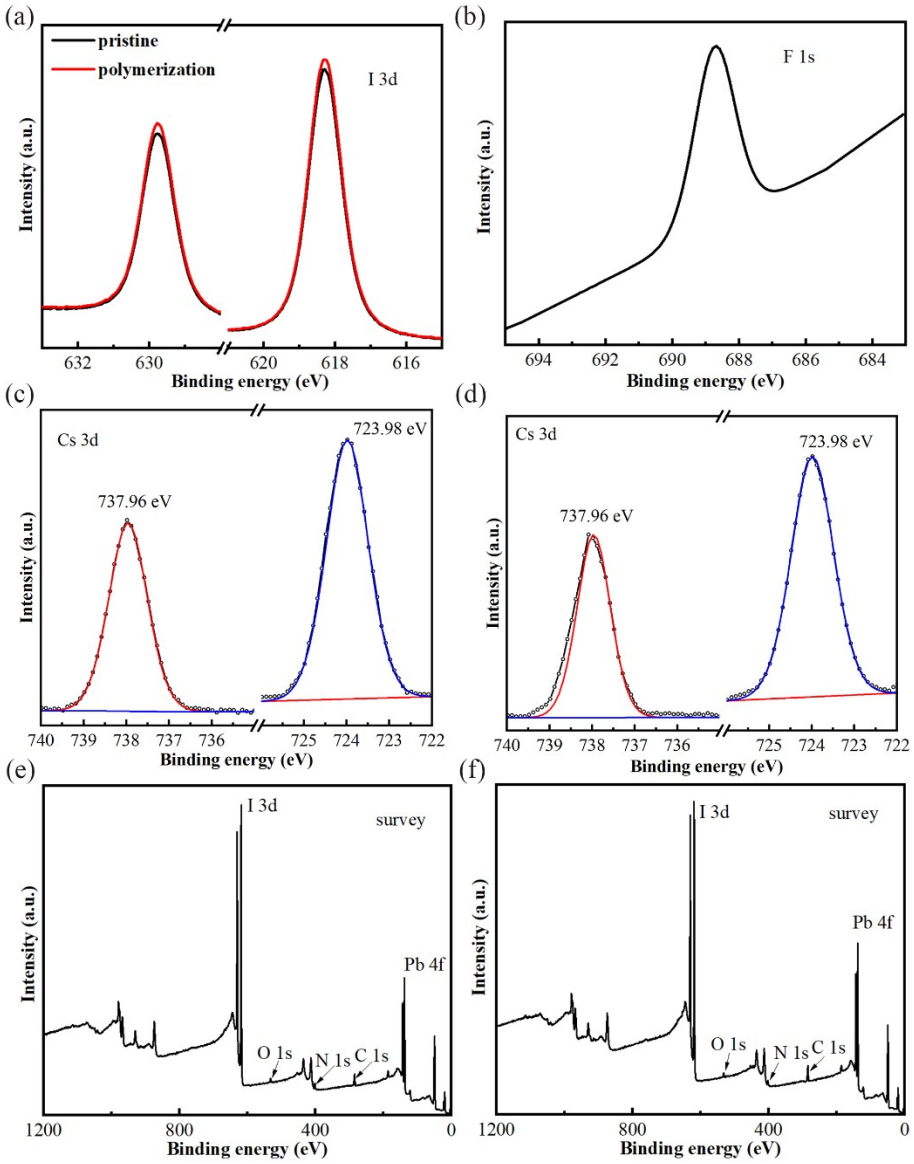

Figure S11. XPS spectra from top-surface of SnO_2 electron transport layer with CsFAMA-based perovskite deposited: (a) I 3d, (b) F 1s core level, Cs 3d of (c) the pristine and (d) the optimized perovskite film, (e) survey (with in-situ polymerization strategy), and (f) survey (for the pristine).

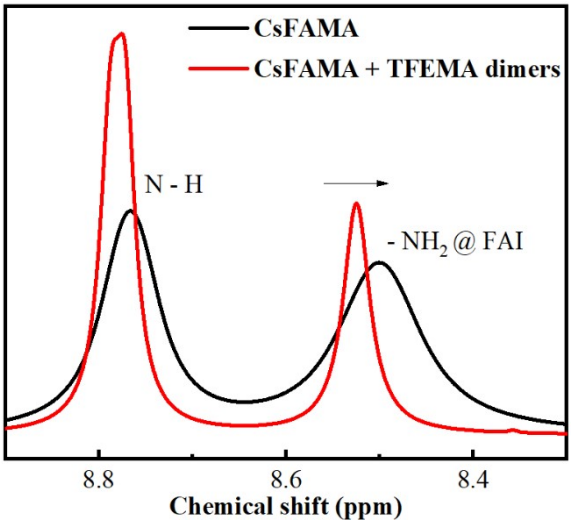

Figure S12. ^{1}H-NMR spectra of N-H and -NH_2 group of FAI.

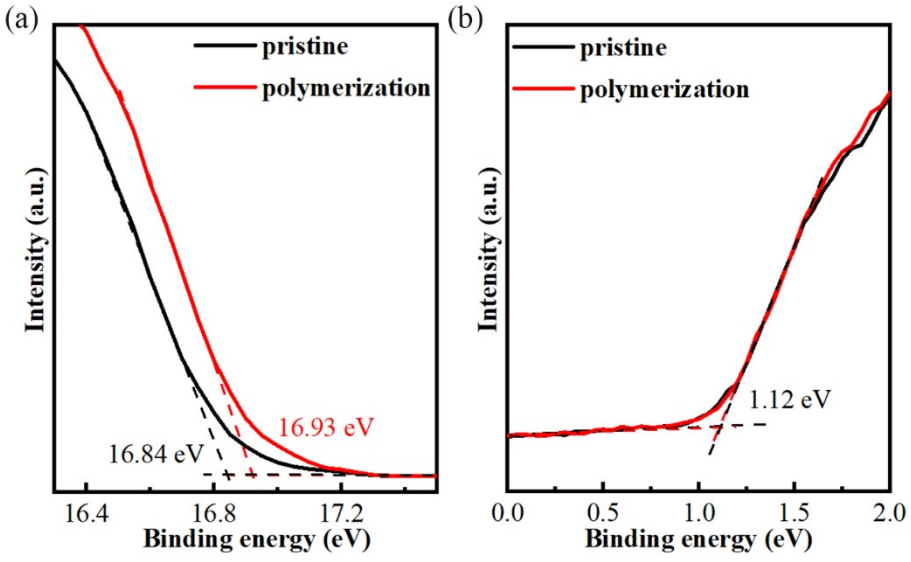

Figure S13. (a) Valence band edges and (b) cutoff regions of UPS spectra for the perovskite films processed with and without an in-situ polymerization strategy.

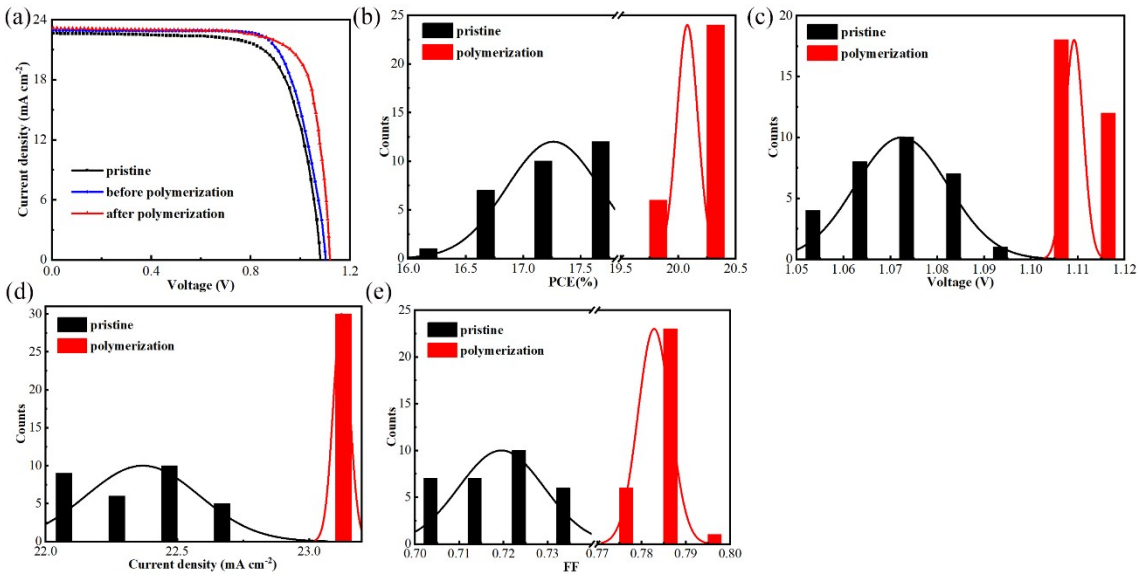

Figure S14. (a) J-V curves for the pristine device and the devices treated by the TFEMA monomers and dimers. Histogram of (b) PCE, (c) V_{oc}, (d) J_{sc}, and (e) FF distribution for solar cells based on the pristine and the crosslinked perovskite devices.

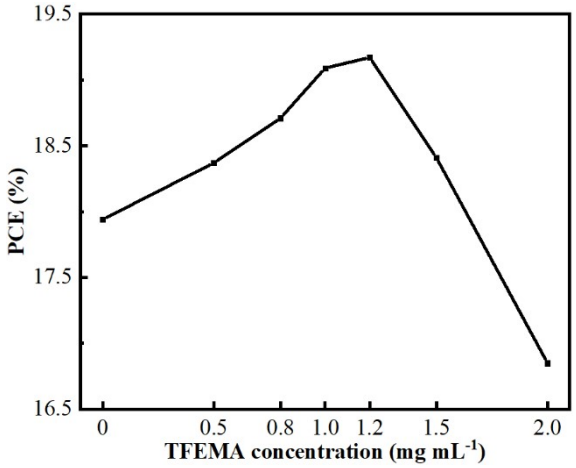

Figure S15. PCE distribution of the PSCs with different concentrations of the TFEMA monomers.

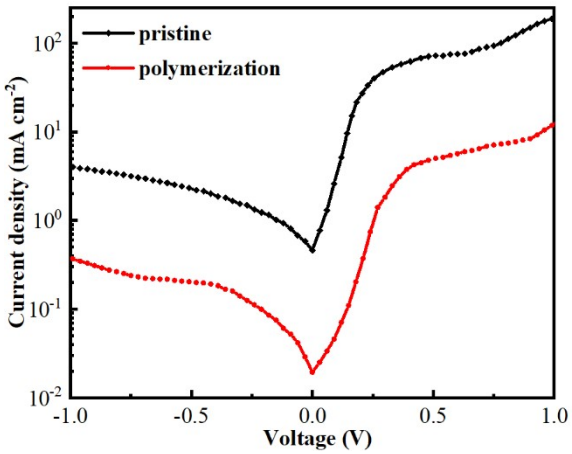

Figure S16. Logarithmic plot of the J-V characteristics of the corresponding devices in the dark.

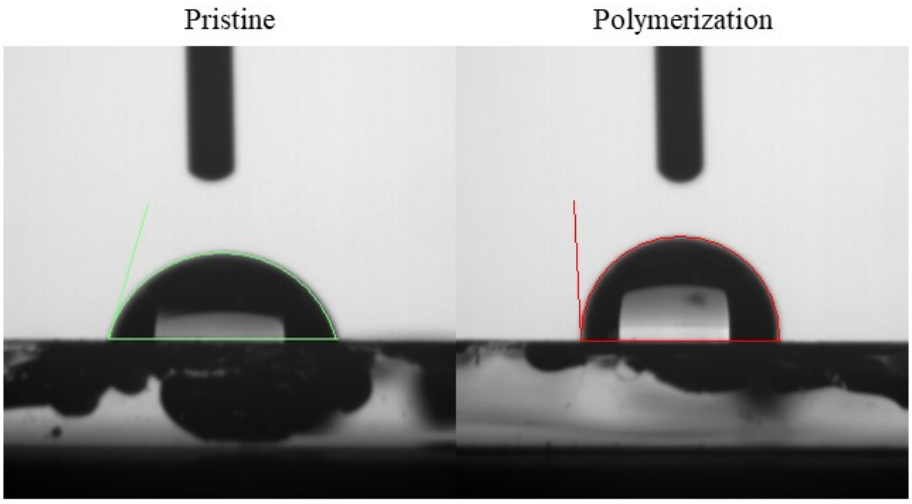

Figure S17. The contact angle between perovskite films (the pristine and optimized device) and water droplets.

Table S1. The detailed PL parameters of the perovskite films with and without an in-situ polymerization process.

Device	A_1	A_2	τ_1 (ns)	τ_2 (ns)	τ_{avg} (ns)
pristine	0.92	0.099	22.35	55.17	29.34
polymerization	0.49	0.54	33.65	72.42	60.92

Table S2. The calculated parameters for the pristine and TFEMA-dimers-modified perovskite active layer.

Sample	E_{cutoff} (eV)	E_{onset} (eV)	W_F (eV)	VBM (eV)	E_g (eV)	CBM (eV)
pristine	16.84	1.12	4.38	5.50	1.60	3.90
polymerization	16.93	1.12	4.29	5.41	1.60	3.81

Table S3. The detailed photovoltaic parameters for the pristine, before cross-linking, and after cross-linking devices.

Device	V_{oc} (V)	J_{sc} (mA cm^{-2})	FF	PCE (%)
pristine	1.08	22.68	0.704	17.24
before polymerization	1.10	22.93	0.760	19.17
after polymerization	1.11	23.16	0.785	20.18

Table S4. Summary of the PSCs fabricated in air condition.

Additive engineering	Perovskite composition	RH (%)	PCE (%)	Moisture stability	Ref.
2-pyridylthiourea	$MAPbI_3$	50-60	18.2	90%, 720 h (50-60%)	[5]
hydrogen iodide	$MAPbI_3$	50	17.2	-	[6]
diiodomethane	$MAPbI_3$	60	16.5	-	[7]
dry-HCl	$MAPbI_3$	30	17.72	-	[8]
MA (ethanol solvent) and MACl	$MAPbI_3$	10-15	20.3	>95%, 1500 h (20%)	[9]
ZnO nanoparticles	$MAPbI_3$	60	18.34	-	[10]
tetrahydrofuran	$MAPbI_3$	50	15	80%, 480 h (50%)	[11]
4-tert-butylpyridine	$MAPbI_3$	50	12.6	about 80%, 168 h (50%)	[12]
4-tert-butylpyridine	$MAPbI_3$	10-50	16.16	80%, 240 h (50%)	[13]
sodium citrate-PEDOT:PSS	$MAPbI_3$	50	19.10	82.7%, 336 h (85%)	[14]
TFEMA dimers	$Cs_{0.05}(FA_{0.83}MA_{0.17})_{0.95}Pb(I_{0.83}Br_{0.17})_3$	20-30	20.18	82.7%, 2400 h (30-40%)	This work

Table S5. The detailed parameters of electrochemical impedance spectroscopy,

charge mobility, and defect density of the PSCs.

Device	R_s (Ω)	R_{ct} (Ω)	electron mobility ($cm^2\ V^{-1}\ s^{-1}$)	defect density (cm^{-3})
pristine	22.97	20609	6.92×10^{-4}	4.75×10^{15}
polymerization	18.89	15341	2.13×10^{-3}	2.74×10^{15}

Notes and References

1. X. L. Zhang, J. D. Zhang, D. Phuyal, J. Du, L. Tian, V. A. Oberg, M. B. Johansson, U. B. Cappel, O. Karis, J. H. Liu, H. Rensmo, G. Boschloo and E. M. J. Johansson, *Adv. Energy Mater.*, 2018, **8**, 1702049.
2. Q. S. Zhou, J. M. Qiu, Y. F. Wang, M. Yu, J. H. Liu and X. L. Zhang, *ACS Energy Lett.*, 2021, **6**, 1596-1606.
3. Z. H. Dai, S. K. Yadavalli, M. Chen, A. Abbaspourtamijani, Y. Qi and N. P. Padture, *Science*, 2021, **372**, 618-622.
4. Z. Liu, F. Cao, M. Wang, M. Wang and L. Li, *Angew. Chem. Int. Ed.*, 2020, **59**, 4161-4167.
5. M. N. Sun, F. Zhang, H. L. Liu, X. G. Li, Y. Xiao and S. R. Wang, *J. Mater. Chem. A*, 2017, **5**, 13448-13456.
6. J. H. Heo, D. H. Song, H. J. Han, S. Y. Kim, J. H. Kim, D. Kim, H. W. Shin, T. K. Ahn, C. Wolf, T. W. Lee and S. H. Im, *Adv. Mater.*, 2015, **27**, 3424-3430.
7. K. Ankireddy, A. H. Ghahremani, B. Martin, G. Gupta and T. Druffel, *J. Mater. Chem. A*, 2018, **6**, 9378-9383.
8. Z. J. Yang, J. L. Pan, Y. Q. Liang, Q. Li and D. S. Xu, *Small*, 2018, **14**, 1802240.
9. X. F. Huang, R. H. Chen, G. C. Deng, F. M. Han, P. P. Ruan, F. W. Cheng, J. Yin, B. H. Wu and N. F. Zheng, *J. Am. Chem. Soc.*, 2020, **142**, 6149-6157.
10. W. T. Wang, J. Sharma, J. W. Chen, C. H. Kao, S. Y. Chen, C. H. Chen, Y. C. Feng and Y. A. Tai, *Nano Energy*, 2018, **49**, 109-116.
11. B. Chaudhary, A. Kulkarni, A. K. Jena, M. Ikegami and T. Miyasaka, *Energy Technol.*, 2020, **8**, 1900990.
12. C. Liu, W. H. Ding, X. Y. Zhou, J. S. Gao, C. Cheng, X. Z. Zhao and B. M. Xu, *J. Phys. Chem. C*, 2017, **121**, 6546-6553.
13. W. H. Chen, L. L. Qiu, Z. S. Zhuang, L. X. Song, P. F. Du, J. Xiong and F. Ko, *J. Power Sources*, 2019, **442**, 227216.
14. P. Y. Zhang, W. H. Chen, X. Yin, L. X. Song, P. C. Jiang, P. F. Du and J. Xiong, *J. Power Sources*, 2021, **507**, 230302.